13

Formation and dynamics of the electron beam in the electron-optical system of a gyrotron taking into account reflection of electrons from the magnetic mirror

© O.I. Louksha, A.G. Malkin, B.R. Apanevich

Peter the Great Saint-Petersburg Polytechnic University,
195251 St. Petersburg, Russia
e-mail: louksha@rphf.spbstu.ru

Received June 26, 2025
Revised August 19, 2025
Accepted September 12, 2025

A new technique for taking into account the surface roughness of the thermionic cathode and the spread of initial thermal velocities when performing trajectory analysis in the electron-optical system of a gyrotron is discussed. Using this technique, the parameters of the helical electron beam in a moderate-power gyrotron of the 4-mm wavelength range are determined. Based on the particle-in-cell method, collective processes in the electron space charge trapped between the cathode and the magnetic mirror are simulated. Threshold excitation conditions and amplitude-frequency characteristics of low-frequency oscillations associated with the development of instability in the trapped space charge are determined. A possible relationship between these oscillations and resonant structures existing in the electron-optical system is discussed.

Keywords: Microwave electronics, gyrotron, helical electron beam, magnetic mirror, low-frequency oscillations.

DOI: 10.61011/TP.2026.02.62893.164-25

Introduction

Gyrotrons are the most effective devices for generating high-power microwave radiation in millimeter and submillimeter wavelength ranges. Plasma heating and control of current in systems designed for controlled nuclear fusion is one of key applications of gyrotrons. Frequency range of $110-170$ GHz is most common for gyrotrons used in modern fusion plants. These gyrotrons can produce megawatt power in quasi-continuous mode with pulse duration up to tens of minutes [1,2]. Besides thermonuclear fusion research, gyrotrons are used in such areas as long-range radiolocation, material processing, high-precision spectroscopy, charged particle acceleration and other modern technologies.

Quality of the electron beam with helical particle trajectories, which is generated in an electron-optical system (EOS) is a key factor of efficiency and maximum permissible parameters of gyrotrons. High quality helical electron beams (HEB) combine high oscillatory electron energy, which is generally characterized by the pitch factor $\alpha = v_\perp/v_\parallel$, where $v_\perp$ and $v_\parallel$ are transverse and longitudinal velocity components with narrow velocity and energy spread and required transverse beam structure (see, for example, [3]). In most cases, electron beam in gyrotrons is generated using a magnetron injection gun (MIG) [4]. The required magnitude of transverse energy is achieved in the magnetic compression region between the gun and resonant cavity where the longitudinal particle energy is transferred into the transverse energy. HEB parameters are determined at the instrument design stage by means of numerical trajectory analysis, which includes calculation of self-consistent particle trajectories in static electric and magnetic fields. Important factors affecting the electron velocity spread in HEB, which shall be considered in such trajectory analysis, include emitting surface roughness of the hot cathode and spread of initial thermal velocities of electrons.

In the presence of velocity spread in HEB, increase in the mean pitch factor of electrons will ultimately lead to a part of beam being reflected from a magnetic barrier and to accumulation of a space charge in a trap between the cathode and barrier. The accumulated space charge is instable, spurious low-frequency oscillations (LFO) may develop in it and affect the quality of primary HEB arriving at the cavity. A number of laboratories conducted theoretical and experimental studies of charge accumulation processes in the trap and spurious LFO properties [3,5–21]. In particular, calculations have shown an important role of secondary emission from the cathode in these processes, a mechanism for electron grouping in the trap, which is responsible for LFO development, has been proposed, methods for decreasing the perturbation rise increment in the accumulated space charge have been defined [7,10,11,13,16,19]. Experiments have identified a possible correlation between the LFO parameters and properties of electrodynamic resonance structures, the function of which is performed by the gyrotron's electron-optical components [8,9,18].

Dynamic processes in the trap are simulated using the particle-in-cell (PIC) method [22]. PIC simulation of long-term processes requires considerable computational burden. To reduce this burden, previous studies used simplified one-dimensional [7,16,17] and two-dimensional [10,11,13]

simulation. However, modern computational systems allow for fully-functional three-dimensional dynamic process simulation with reasonable machine time consumption for large time intervals consisting of hundreds of single particle oscillation periods in the trap. Such simulation can obviously identify the correlation between LFO properties and parameters of gyrotron EOS resonance structures.

Three-dimensional numerical simulation considering reflection of a part of HEB from the magnetic barrier was performed in this work for SPbPU's gyrotron with an operating frequency of 74.2 GHz and microwave power output of about 100 kW [12,20,23]. Previous experiments with this gyrotron have investigated in detail LFO properties, determined their effect on HEB parameters and proposed suppression methods. All calculations in this work were performed in CST Studio Suite [24]. Some features of the employed computational models are described in [25,26].

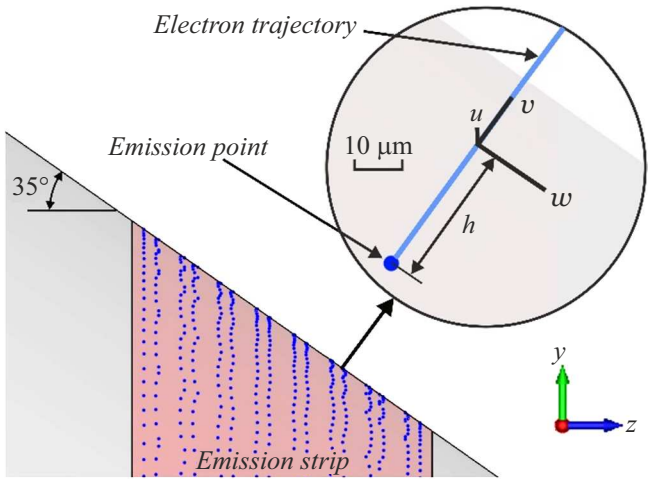

Figure 1. Image of emission centers on the cathode emission strip and close-up — one of the electron trajectories.

1. Consideration of initial electron velocity spread in gyrotron EOS trajectory analysis

Quality of HEB generated in the gyrotron EOS is considerably affected by the initial electron velocity spread resulting from the thermal velocity spread, which occurs when electrons leave the cathode surface, and from roughness of this surface [3,26–28]. Typical size of such roughnesses is from some microns to tens of microns. With such sizes of roughnesses, their effect on the electron velocity spread in HEB is much higher than that of the thermal velocity spread. There are obvious difficulties with the trajectory analysis in EOS with a length of hundreds of millimeters, if the cathode surface has micron-size nonuniformities. Various algorithms have been proposed for considering the initial velocity spread in electron trajectory calculation in a smooth-cathode gyrotron model [27,28]. Work [26] has shown that a transverse velocity spectrum in the cathode model with micron-size hemispheres has a shape close to a velocity spectrum for a smooth cathode, if the Maxwellian distribution of initial velocities was set for it using tools available in CST Studio Suite when setting thermionic emitter properties. For the transverse velocity spread to be close to the experimental one, effective temperature, as a parameter of this distribution, shall be significantly higher than typical hot cathode temperatures. However, in such simplest method of setting thermoelectronic emission properties, electrons starting from the cathode will have abnormally high initial energy (total velocity), which doesn't meet the real conditions. This causes spurious electron energy spread in HEB and prevents from correct calculation of particle accumulation processes in the gyrotron trap when reflecting a part of beam from the magnetic barrier within the PIC simulation.

Approach proposed in [26] has been corrected in this work to avoid the spurious spread of initial energies on cathode. Procedure for considering initial velocities included several stages.

Stage I. For the electron-optical system model with the chosen meshing and operating mode, which were not changed later, electron trajectories for initial electron energy on cathode equal to zero were calculated in Tracking Solver tool. Time dependences of the global coordinates $x(t)$, $y(t)$, $z(t)$ and velocities $v_x(t)$ were determined for each trajectory within simulation data post-processing. $v_y(t)$, $v_z(t)$.

Stage II. Time t_0, for which electron trajectory rise above the cathode surface was $h \approx 30\,\mu$m, was chosen. Note that calculations in the cathode model with hemispheres with radius r_0 regularly spaced on the cathode surface showed that transverse velocity distribution of electrons was almost unchanged as the distance from the cathode increased, if this distance was larger than approx. $2 \cdot r_0$ [26]. However, at $r_0 = 14\,\mu$m, velocity spreads obtained from the calculations and experiments with SPbPU's gyrotron were approximately equal. Current calculations determined $x(t_0)$, $y(t_0)$, $z(t_0)$, $v_{x0}(t_0)$, $v_{y0}(t_0)$, $v_{z0}(t_0)$ for each electron trajectory. These values were used to calculate the total velocity $v_{abs}(t_0)$, and velocity components along the axes of the local coordinate system $v_{u0}(t_0)$ and $v_{w0}(t_0)$ (Figure 1). The u axis is directed azimuthally, the w axis is directed along the cone cathode generatrix and the v axis is normal to the cathode surface. Direction of the u, w and v axes will be obviously different for each trajectory.

Stage III. Random tangential components of the initial velocity $v'_u(t_0)$ and $v'_w(t_0)$ were set on the assumption that these velocities are distributed in accordance with the Gaussian function:

$$f(v) = \left(\frac{1}{2\pi}\right)^{1/2} \frac{1}{\sigma} \exp\left(-\frac{v^2}{2\sigma^2}\right),$$

where σ is the mean-square deviation. Two values of $v'_u(t_0)$ and two values of $v'_w(t_0)$ with of different sign

before the magnitude of velocity were determined for each electron trajectory. The Box–Muller transform was used for setting the pairs of normally distributed random velocities [29]. Hereinafter, $W_{\text{init}}[eV] = \frac{m \cdot \sigma^2}{e}$, where e and m are the electron charge and mass, will be used as a parameter characterizing the initial velocity spread.

Stage IV. New velocities along the local coordinate axes were equal to:

$$v_{u1}(t_0) = v_{u0}(t_0) + v'_u(t_0),$$

$$v_{w1}(t_0) = v_{w0}(t_0) + v'_w(t_0),$$

$$v_{v1}(t_0) = \sqrt{v^2_{\text{abs}}(t_0) - v^2_{u1}(t_0) - v^2_{w1}(t_0)}.$$

These values were used to determine new global initial velocities $v_{x1}(t_0)$, $v_{y1}(t_0)$, $v_{z1}(t_0)$. $x(t_0)$, $y(t_0)$, $z(t_0)$, $v_{x1}(t_0)$, $v_{y1}(t_0)$, $v_{z1}(t_0)$ data array formed the particle inlet interface for the trajectory analysis in the smooth-cathode EOS model with the initial electron velocity spread. Two particles with different velocities are emitted from each emission center in this interface.

The above-mentioned procedure was implemented in CST Studio Suite macro.

2. Trajectory analysis in the gyrotrone electron-optical system

First of all, statistical electron trajectories were calculated using Tracking Solver. These calculations used the total EOS model with electron beam deposition on a collector. HEB was formed using a standard MIG without a control electrode, with angle between the cathode cone generatrix and axis equal to 35° [26,30]. Electron source consisted of 10 960 emission centers evenly spaced on the cone cathode band. Emission was azimuthally uniform. Tetrahedral meshing with a smaller mesh interval in the emitter area and in the electron trajectory area was used. The total amount of meshes was approx. 39 million.

Design operating mode of the gyrotron is characterized by the following values of the main parameters: accelerating voltage $U_0 = 30$ kV, beam current $I_b = 10$ A, magnetic field in the center of cavity $B_0 = 2.75$ T, magnetic compression coefficient $B_0/B_c = 18.0$ [12,25,26,30]. $B_0/B_c = 18.0$ corresponds to 24 cathode coil turns of SPbPU's experimental gyrotronSPbPU [23]. In this mode, the mean pitch factor $\alpha = v_\perp/v_\parallel$ and transverse velocity spread $\delta v_\perp$ calculated without the initial velocity spread were equal to 1.29 % and 6.1 %, respectively. Velocity spread in this work was determined as a mean-square deviation from the mean velocity. α and $\delta v_\perp$ were recorded in the central plane of the cavity $z = 260.5$ mm in the longitudinal magnetic field distribution maximum $B(z)$ ($z = 0$ — central plane of the cathode emission band). When the initial spread was added, broadening of the transverse electron velocities in the beam and some increase in the mean pitch factor were observed. For example, at $W_{\text{init}} = 7.15$ eV, the mean pitch factor was equal to 1.33, and the transverse velocity spread was 8.8 %. Such spread was obtained earlier in experiments with SPbPU's gyrotron [20,26]. Electron distributions by transverse velocity $v_\perp$ and total velocity v_{abs} for the given modes are shown in Figure 2. For the chosen histogram interval width equal to $7.2 \cdot 10^5$ m/s, total velocity spectra for these modes coincide. These spectra feature small spread $\delta v_{abs} = 0.052$ % for $W_{\text{init}} = 0$ and $\delta v_{abs} = 0.053$ % for $W_{\text{init}} = 7.15$ eV. The figure also shows v_0 of electron with energy 30 keV. Difference between v_{abs} and v_0 characterizes the beam potential sag in the central plane of the cavity.

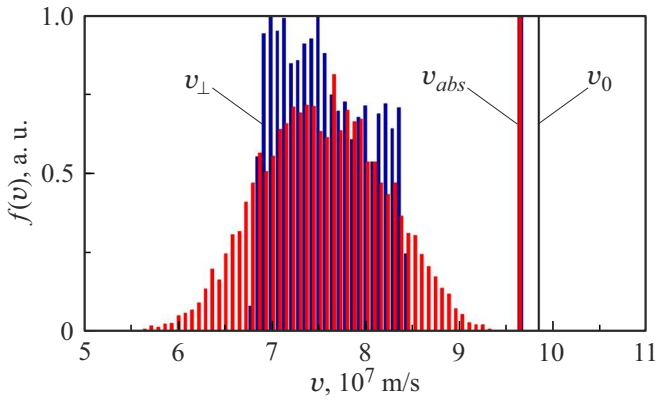

Figure 2. Electron distributions by transverse velocity $v_\perp$ and total velocity v_{abs} without the initial velocity spread (blue) and with the initial velocity spread corresponding to $W_{\text{init}} = 7.15$ eV (red). v_0 of electron with energy 30 keV is shown.

In the given mode, transverse velocities of all particles in the distribution maximum $B(z)$ are lower than the total velocity (Figure 2), i.e. there is no particle reflection from the magnetic barrier. However, as the mean pitch factor and/or velocity spread in HEB increase, reflected particles inevitably occur and, as mentioned above, can be accumulated in the trap between the cathode and magnetic barrier. The reflection coefficient of electrons from the barrier R, from which the rate of electron entry into the trap depends, can obviously change as the space charge accumulated in this trap increases.

To increase the mean pitch factor of electrons in HEB and implement the modes with electron reflection from the barrier, the magnetic compression coefficient was increased to $B_0/B_c = 19.7$. This value corresponds to 21 cathode coil turns of SPbPU's gyrotron [23]. Some simplification of the gyrotron EOS model was also accomplished. EOS length was limited by the plane $z = 274.5$ mm coinciding with the end of the regular part of the cavity. This plane included a „magnetic wall", on which there was no tangential magnetic field component. Transition to 0.8 mm hexahedral meshing was made and gave a total of 7.9 million meshes. This EOS model was also used in the PIC simulation described below in Section 3. The simplifications made it possible to reduce the time of this simulation.

HEB parameters calculated with electron reflection from the magnetic barrier ($B_0/B_c = 19.7$)

U_0, kV	α	$\delta v_\perp$, %	R_0, %
28	2.01	6.23	0.78
30	2.42	5.30	1.56
32	2.82	4.28	4.14
34	3.22	3.53	8.59
36	3.51	3.13	14.64

When particles are reflected from the magnetic barrier and then reflected again in the cathode area, then achievement of the convergence condition for the self-consistency trajectory calculation in Tracking Solver cannot be ensured. Nevertheless, we used this solver to calculate the „initial" reflection coefficient R_0, when the effect of charge of reflected particles on the trajectory of the initial beam passing through the barrier towards the cavity was still low. For this, the simulation time, or the number of time intervals in particle trajectory calculation, was set to the lowest value, at which, however, all initial beam particles could reach the outlet plane $z = 274.5$ mm. In this case, trapped particles have maximum one reflection in the magnetic barrier area. For calculations with reflection of a part of HEB and accumulation of space charge in the trap, approach to considering the initial velocity spread described in Section 1 prevents from calculating the particle trajectories correctly. Therefore, the results given below were obtained at the initial particle energy on cathode equal to zero. The number of emission centers was equal to 10 960 as before.

The table shows calculated mean pitch factor α and velocity spread $\delta v_\perp$ in the initial beam recorded in the central plane of the cavity $z = 260.5$ mm, and initial reflection R_0 at various values of accelerating voltage U_0. The calculated values of R_0 are much lower than the reflection coefficient for the Gaussian distribution $f(v_\perp)$ at the same α and $\delta v_\perp$ [16]. This is due to the fact that the transverse velocity spectra in these calculations, similar to that shown in Figure 2, had a quite sharp decay of $f(v_\perp)$ at high $v_\perp$ compared with the Gaussian distribution. At $U_0 = 30$ kV, the mean electron transit time of the initial HEB electrons from the cathode to the plane $z = 260.5$ mm was equal to approx. 4.5 ns, and the total charge of all particles in the model was equal to $5.1 \cdot 10^{-8}$ C.

3. PIC- simulation of dynamic processes with electron reflection from the magnetic barrier

EOS model, for which PIC simulation was performed, is shown in Figure 3. This model had waveguide ports in both end planes $z = -90$ mm and 274.5 mm, through which

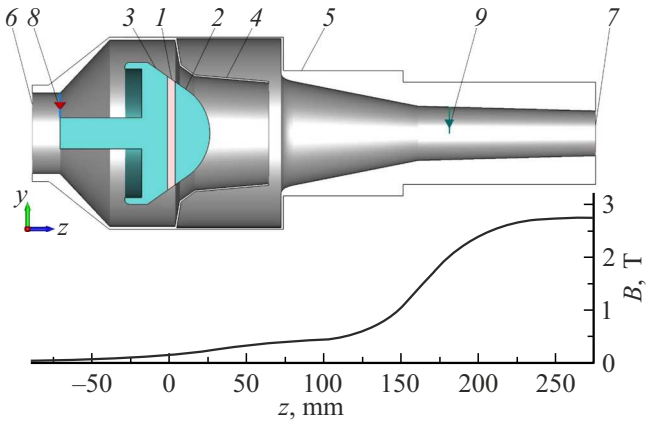

Figure 3. Schematic diagram of the gyrotron EOS model: *1* — emission band, *2* — cathode front side, *3* — cathode rear side, *4* —anode, *5* — housing, *6*, *7* — waveguide ports, *8* — discrete port, *9* — voltage monitor of the plane $z = 180$ mm. Longitudinal distribution of the magnetic field induction $B(z)$ on the axis ($r = 0$) is shown.

high-frequency signals were output from the model without reflection. Difference of potentials between the cathode and anode was created through a discrete linear port used in CST Studio Suite for setting the voltage between two points in the model. This voltage was gradually increasing from 0 to U_0 during the first ~ 50 ns, after which it remained unchanged. Port impedance was equal to 50 Ω. As the voltage increased, thermal emission current from cathode increased. The voltage and current pulse amplitude rise rate obviously affects the processes in the trap at the initial simulation stage [31]. It is important to ensure gradual voltage and current rise to avoid any significant effect of the beam „head" on conditions of charge accumulation and grouping in the trap.

Note that the secondary emission from the cathode plays an important role in the gyrotron EOS electronic processes during particle reflection from the magnetic barrier, creating, in particular, additional channel for particle entry into the trap (see, for example, [10]). CST Studio Suite has tools for taking into account emission of secondary electrons during bombardment of EOS components, including the extensive materials library. Molybdenum with the maximum secondary emission coefficient of 1.23 at the incident electron energy of 600 eV was chosen as a cathode unit material, excluding the emission band [32]. Secondary emission data corresponding to a W-Ba impregnated cathode with the maximum coefficient of 2.5 and energy of 1000 eV [33]. An ideal conductor was chosen as the material for other EOS components. The number of emission centers on the cathode was reduced to 480. Simulation time interval was approximately equal to $1 \cdot 10^{-3}$ ns. Simulation time was set to 3000 ns, which corresponds to approximately $300 - 400$ oscillation periods of a single particle between the cathode and magnetic barrier. In this case, by the end of simulation, the total number of large particles was equal to $(1 - 2) \cdot 10^7$.

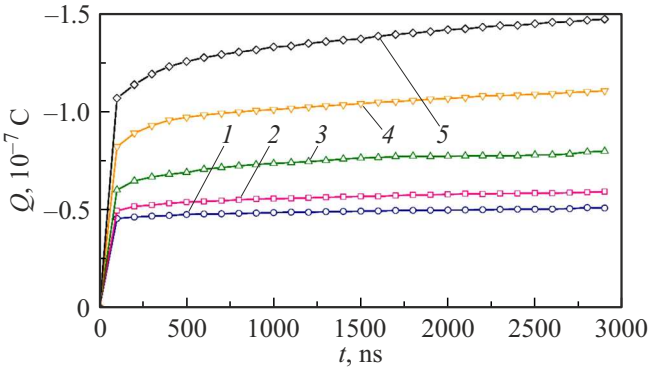

Figure 4. Time dependences of the total particle charge $Q(t)$ at different values of U_0: 28 (*1*), 30 (*2*), 32 (*3*), 34 (*4*), 36 kV (*5*).

With such settings, calculation time for one problem was several days using an accelerator and SPbPU supercomputer center. The model included dedicated monitors used in CST Studio Suite for recording various parameters during simulation and subsequent analysis of these parameters. The monitors recorded currents to EOS electrodes, voltages between the instrument housing and chosen points in the working space, and parameters of large particles in various cross-section planes.

Dependences of the total particle charge throughout the simulation domain on time for different values of U_0 are shown in Figure 4. It can be seen that the charge increases gradually with time during the entire simulation period $t = 3000$ ns. The increase rate obviously depends on the coefficient of electron reflection from the barrier, which increases as U_0 grows. Thus, a quasi-steady state, at which the particle flows to and from the trap are equal on average, was not achieved even with a high reflection coefficient ($U_0 = 36$ kV) where intense oscillations develop in the accumulated charge (see below).

Currents recorded in the circuits of various EOS electrodes vary with time. Corresponding dependences for the maximum voltage $U_0 = 36$ kV are shown in Figure 5. Maximum current to the emission band I_1 is achieved at the beginning of simulation after the transition stage at the leading edge ($t \approx 50$ ns). Then, the current to the band decreases with time, but the current to the cathode rear side I_2 and to the anode I_4 increases, which is associated with the trapped electron diffusion towards larger radii. Similar dependences were also observed in previous calculations (for example, [10,13,19,21]). Current to the cathode front side I_3 was negligibly low compared with currents to other electrodes. Due to a high coefficient of secondary emission from the band, it is secondary electrons from this electrode that give the greatest contribution to the total beam current. This leads to approximately the same time behavior of I_1 and $I_5$of the beam passing through the magnetic barrier and recorded at the outlet interface. At the and of simulation $t = 3000$ ns, I_5 was approximately 5 % as high as the thermoelectronic emission current from the cathode set to 10 A.

The space charge accumulated in the trap is concentrated in the area between the cathode and magnetic barrier. Figure 6 shows linear charge density λ calculated as integral of the volume charge density ρ on the cross-section plane depending on the z coordinate of this plane for different times t at $U_0 = 36$ kV. Similar to one-dimensional simulation [23], distribution maxima $\lambda(z)$ are shifted to each other as the charge is getting accumulated in the trap. In other words, the „effective“ trap length averaged over the whole ensemble of particles becomes smaller.

Voltage monitor mounted in the cross-section plane $z = 180$ mm, recorded the difference of potentials U_{180} between a point on the instrument axis ($r = 0$) and grounded housing (Figure 3). Dependences $U_{180}(t)$ calculated at different voltages U_0 are shown in Figure 7. At low voltages $U_0 = 28$, 30 and 32 kV, there were no signals indicating that regular oscillations develop in the space charge accumulated in the trap. Such oscillations with f_{LFO} approximately equal to 53 MHz can be seen on $U_{180}(t)$ for $U_0 = 36$ kV. They appeared at $t \approx 1000$ ns and reached saturation in amplitude approximately after 1500 ns, which corresponds to ~ 80

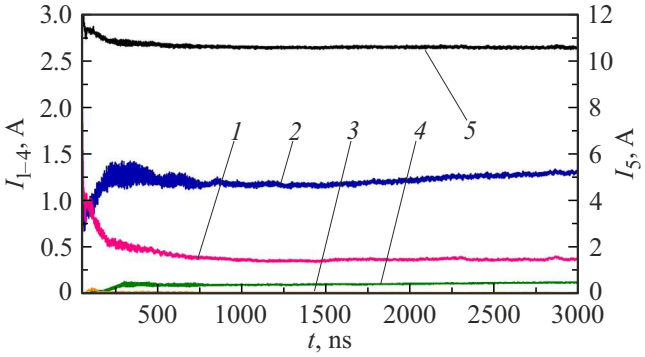

Figure 5. Dependences of currents to the gyrotron EOS components on time at $U_0 = 36$ kV: *1* — emission band, *2* — cathode unit rear side, *3* — cathode unit front side, *4* — anode, *5* — outlet front side $z = 274.5$ mm.

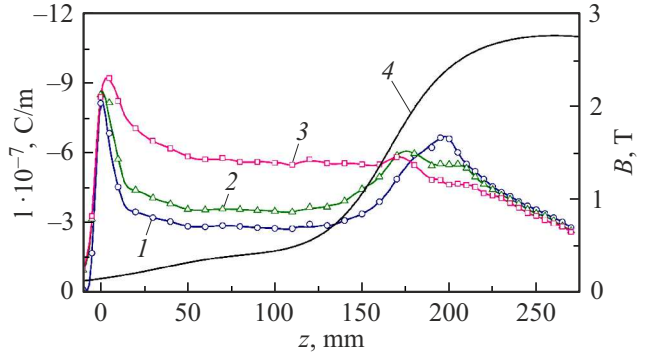

Figure 6. Distributions of the linear density of space charge λ along the longitudinal coordinate z at $U_0 = 36$ kV for various times t: 100 (*1*), 300 (*2*), 2900 ns (*3*); *4* — longitudinal distribution of magnetic field induction $B(z)$ on the axis ($r = 0$).

oscillation periods. Such perturbation rise increments in the space charge in the trap were reported earlier for one-dimensional simulation [16].

Judging by f_{LFO}, it is suggested that one electron bunch oscillates in the trap in this mode. This is confirmed by comparing signal phases from the voltage monitors mounted in the planes with different values of the longitudinal z coordinate. Space charge grouping in the trap, as has been shown earlier [16,23], may be attributed to non-isochronism of particle oscillations between reflection planes at the cathode and magnetic barrier. f_{LFO} in this case is defined by the shape of a kind of potential well for oscillating particles, which depends on the magnetic field distribution and electric field distribution that varies as the space charge is getting accumulated in the trap.

With lower voltage $U_0 = 34$ kV and, consequently, lower particle flow to the trap compared with $U_0 = 36$ kV, low-amplitude signals were observed at the end of simulation time approximately at 150 MHz (Figure 7). Such frequency suggests that three oscillating bunches may exist simultaneously in the trap. Manyfold increase in the LFO frequency with decreasing coefficient of reflection from the barrier has been observed earlier in one-dimensional simulation [16,23]. Generally, in transition from one-dimensional to three-dimensional simulation, threshold coefficients of reflection from the magnetic barrier and space charge accumulated in the trap, at which regular LFOs appeared, increased significantly. This difference was possibly caused by relatively small amount of large particles, into which the electron beam is broken, in three-dimensional simulation. Increase in this amount is, unfortunately, limited by computational resources.

Correlation between LFO in the electron cloud and two types of resonance structures in the gyrotron EOS: a resonant cavity and equivalent oscillatory circuit (distributed LC circuit), turns out to be possible. Calculations of eigen modes in this EOS model using Eigenmode Solver have shown that resonance frequencies of all modes exceed 1 GHz, i.e. are much higher than f_{LFO}. Any „reference“ of signal frequency in the electron space charge to the frequencies of these modes wasn't noted. The distributed LC circuit was formed using the discrete port inductance and cathode-anode gap capacity. In this model, its resonance frequency was within the range of hundreds of megahertz. This frequency and Q factor of the LC circuit could be varied by modifying the EOS component configurations, discrete port dimensions or during absorber installation. Unless the discrete port impedance was set specifically, the current signals to the EOS electrodes contained high-frequency components at the LC circuit resonance frequency. Amplitude of these components grew as the space charge accumulated in the trap increased with rising U_0. However, by introducing an impedance of 50 Ω into the discrete port, signals related to the LC circuit excitation were suppressed. Such LC circuits related to the electron beam may also exist in a real instrument. In case of such correlation, „reference“ of the LFO frequency to the resonance frequency of this circuit is possible (see, for example, [9]). Decrease in the Q factor of the LC circuit in this case can make it possible to reduce the spurious LFO intensity in the instrument.

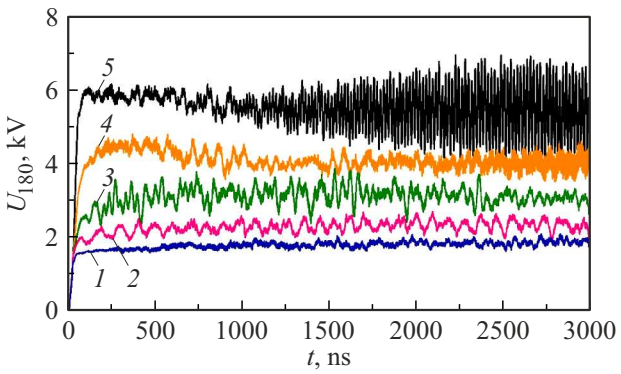

Figure 7. Time dependences of U_{180} on the instrument axis ($r = 0$) in the cross-section plane $z = 180$ mm at different accelerating voltages U_0: 28 (*1*), 30 (*2*), 32 (*3*), 34 (*4*), 36 kV (*5*).

Conclusion

Trajectory analysis in EOS of SPbPU's gyrotron has been performed using a new procedure for considering the initial electron velocity spread caused by hot cathode surface roughness and thermal velocity spread. The trajectory analysis data were used to choose gyrotron operating modes where a part of the e;ectron beam is reflected from the magnetic barrier.

Three-dimensional PIC simulation of electron space charge accumulation and dynamics in the trap between the cathode and magnetic barrier was performed in these modes. It is shown that spurious low-frequency oscillations caused by charge grouping into longitudinally oscillating bunches can occur. These oscillations occur at much higher coefficient of reflection from the magnetic barrier compared with the previous one-dimensional PIC simulation, which may be associated with relatively „coarse“ breakdown of the flow into large particles in one-dimensional simulation. Special focus in the calculations was made on the correlation between the spurious oscillation characteristics and parameters of resonance structures existing in the gyrotron EOS. Effect of the LC circuit formed by the gun electrodes and voltage source on the dynamic processes in the electron beam was detected. The effect of this circuit could be avoided by means of reducing its Q factor with introduction of additional resistance.

Acknowledgments

Some of the results were obtained using the computational resources of the supercomputer center at Peter the Great St. Petersburg Polytechnic University (http://www.scc.spbstu.ru). The authors appreciate the assistance provided by P.A.Trofimov in discussing the findings.

Conflict of interest

The authors declare no conflict of interest.

References

[1] M.K.A. Thumm, G.G. Denisov, K. Sakamoto, M.Q. Tran. Nuclear Fusion, **59** (7), 073001 (2019). DOI: 10.1088/1741-4326/ab2005

[2] A.G. Litvak, G.G. Denisov, V.E. Myasnikov, E.M. Tai, E.A. Azizov, V.I. Ilin. J. Infrared Millimeter Terahertz Waves, **32** (3), 337 (2011). DOI: 10.1007/s10762-010-9743-8

[3] Sh.E. Tsimring. *Electron Beams and Microwave Vacuum Electronics* (John Wiley & Sons, Inc., Hoboken, New Jersey, 2007)

[4] A.L. Gol'denberg, M.I. Petelin. Radiophys. Quant. Electron. **16** (1), 106 (1973). DOI: 10.1007/BF01080801

[5] V.E. Zapevalov, V.N. Manuilov, Sh.E. Tsimring. Radiophys. Quant. Electron., **33** (12), 1043 (1990). DOI: 10.1007/BF01040147

[6] O.I. Louksha, G.G. Sominskii. Tech. Phys., **39** (11), 1173 (1994).

[7] D.V. Borzenkov, O.I. Luksha. Tech. Phys., **42** (9), 1071 (1997). DOI: 10.1134/1.1258768

[8] I. Gorelov, J.M. Lohr, D. Ponce, R.W. Callis, H. Izeki, R.A. Legg, S.E. Tsimring. In: *Proc. 24th Int. Conf. Infrared and Millimeter Waves* (Monterey, USA, 1999), TU-D8

[9] B. Piosczyk, A. Arnold, G. Dammertz, O. Dumbrajs, M. Kuntze, M.K. Thumm. IEEE Trans. Plasma Sci., **30** (3), 819 (2002). DOI: 10.1109/TPS.2002.1010853

[10] P.V. Krivosheev, V.N. Manuilov. Prikladnaya fizika, **3**, 80 (2002) (in Russian).

[11] P.V. Krivosheev, V.N. Manuilov. Prikladnaya fizika, **1**, 101 (2004) (in Russian).

[12] O. Louksha, B. Piosczyk, G. Sominski, M. Thumm, D. Samsonov. IEEE Trans. Plasma Sci., **34** (3), 502 (2006). DOI: 10.1109/TPS.2006.875779

[13] V.N. Manuilov. Radiophys. Quant. Electron., **49** (10), 786 (2006). DOI: 10.1007/s11141-006-0113-2

[14] E.V. Ilyakov, I.S. Kulagin, V.N. Manuilov, A.S. Shevchenko. Radiophys. Quant. Electron., **51** (10), 772 (2008). DOI: 10.1007/s11141-009-9080-8

[15] A.J. Cerfon, E. Choi, C.D. Marchewka, I. Mastovsky, M.A. Shapiro, R.J. Temkin. IEEE Trans. Plasma Sci., **37** (7), 1219 (2009). DOI: 10.1109/TPS.2009.2020903

[16] O.I. Louksha. Radiophys. Quant. Electron., **52** (5–6) 386 (2009). DOI: 10.1007/s11141-009-9149-4

[17] R. Yan, T.M. Antonsen, G.S. Nusinovich. IEEE Trans. Plasma Sci., **38** (6), 1178 (2010). DOI: 10.1109/TPS.2010.2045160

[18] T. Rzesnicki, B. Piosczyk, S. Kern, S. Illy, J. Jin, A. Samartsev, A. Schlaich, M. Thumm. IEEE Trans. Plasma Sci., **38** (6), 1141 (2010). DOI: 10.1109/TPS.2010.2040842

[19] V.N. Manuilov, A.A. Mazur. Vestnik Nizhegorodskogo un-ta im. N.I. Lobachevskogo, **5** (3), 327 (2011) (in Russian).

[20] O.I. Luksha, D.B. Samsonov, G.G. Sominsky, S.V. Semin. ZhTF, (in Russian). **83** (5), 132 (2013).

[21] I.Gr. Pagonakis, B. Piosczyk, J. Zhang, S. Illy, T. Rzesnicki, J.-P. Hogge, K. Avramidis, G. Gantenbein, M. Thumm, J. Jelonnek. Phys. Plasmas, **23**, 023105 (2016). DOI: 10.1063/1.4941705

[22] Ch. Bedsel, A. Lengdon. *Fizika plazmy i chislennoe modelirovanie* (Energoatomizdat, M., 1989) (in Russian).

[23] O.I. Luksha. *Vintovye elektronnye potoki girotronov: dinamika prostranstvennogo zaryada i metody povysheniya kachestva* (in Russian) (Dokt. diss. 01.04.04 / SPbPU, SPb., 2011)

[24] *CST Studio Suite. Electromagnetic field simulation software* Electronic resource. Available at: https://www.3ds.com/products-services/simulia/products/cst-studio-suite/

[25] O.I. Louksha, P.A. Trofimov. Tech. Phys., **64** (12), 1889 (2019). DOI: 10.1134/S1063784219120156

[26] O.I. Louksha, P.A. Trofimov, A.G. Malkin. Radiophys. Quant. Electron., **65**, 209 (2022). DOI: 10.1007/s11141-023-10206-6

[27] K.A. Leshcheva, V.N. Manuilov. UPF, **7** (3), 298 (2019) (in Russian).

[28] J. Zhang, S. Illy, I.Gr. Pagonakis, K.A. Avramidis, M. Thumm, J. Jelonnek. Nucl. Fusion, **56** (2), Art. 026002 (2016). DOI: 10.1088/0029-5515/56/2/026002

[29] G.E.P. Box, M.E. Muller. Ann. Math. Stat., **29** (2), 610 (1958). DOI: 10.1214/aoms/1177706645

[30] O.I. Louksha, P.A. Trofimov. Tech. Phys., **63** (4), 598 (2018). DOI: 10.1134/S106378421804014X

[31] V.N. Manuilov, V.G. Pavel'ev. Radiophys. Quant. Electron., **51**, 384 (2008). DOI: 10.1007/s11141-008-9038-2

[32] I.S. Grigoryev, E.Z. Mejlikhov (red.). *Fizicheskie velichiny.* Spravochnik (Energoatomizdat, M., 1991) (in Russian).

[33] R.E. Thomas, C.D. Morrill. In: *Applications of Surface Science* (Amsterdam, North Holland, 1983), p. 292.

Translated by E.Ilyinskaya